f-wave superfluidity from repulsive interaction in Rydberg-dressed Fermi gas

Ahmet Keleş,[1,2] Erhai Zhao,[2] and Xiaopeng Li[3,*]

[1] Department of Physics and Astronomy, University of Pittsburgh, Pittsburgh, Pennsylvania 15260, USA
[2] Department of Physics and Astronomy, George Mason University, Fairfax, Virginia 22030, USA
[3] State Key Laboratory of Surface Physics, Institute of Nanoelectronics and Quantum Computing, & Department of Physics, Fudan University, Shanghai 200433, China

Interacting Fermi gas provides an ideal model system to understand unconventional pairing and intertwined orders relevant to a large class of quantum materials. Rydberg-dressed Fermi gas is a recent experimental system where the sign, strength, and range of the interaction can be controlled. The interaction in momentum space has a negative minimum at q_c inversely proportional to the characteristic length-scale in real space, the soft-core radius r_c. We show theoretically that single-component (spinless) Rydberg-dressed Fermi gas in two dimensions has a rich phase diagram with novel superfluid and density wave orders due to the interplay of the Fermi momentum p_F, interaction range r_c, and interaction strength u_0. For repulsive bare interactions $u_0 > 0$, the dominant instability is f-wave superfluid for $p_F r_c \lesssim 2$, and density wave for $p_F r_c \gtrsim 4$. The f-wave pairing in this repulsive Fermi gas is reminiscent of the conventional Kohn-Luttinger mechanism, but has a much higher T_c. For attractive bare interactions $u_0 < 0$, the leading instability is p-wave pairing. The phase diagram is obtained from functional renormalization group that treats all competing many-body instabilities in the particle-particle and particle-hole channels on equal footing.

I. INTRODUCTION

Understanding the many-body instabilities and symmetry breaking in strongly interacting fermions in two-dimension (2D) holds the key to several long-standing problems in condensed matter physics. One example is the precise mechanism by which unconventional superconductivity with various pairing symmetries emerges from repulsive interactions, in materials ranging from cuprate [1], ruthenate [2], and pnictide [3] superconductors. These and other correlated quantum materials typically display intertwined vestigial orders, e.g. in the so-called pseudogap region where charge density waves, pairing, and other fluctuations compete. Recently, ultracold Fermi gases [4, 5] of atoms and molecules have become a promising experimental platform to tackle some of these open problems by realizing Hamiltonians such as the Fermi-Hubbard model [6–8] with tunable interactions [9]. This offers opportunity to deepen our understanding of the “pairing glue” in repulsively interacting systems, and shed light on the complex interplay of quantum fluctuations in distinct channels for simple and highly controlled Hamiltonians. In this paper, we show theoretically that Rydberg-dressed Fermi gas of alkali atoms with tunable long-range interactions gives rise to not only p-wave topological superfluids for attractive bare interactions, but also f-wave superfluid with high transition temperatures stemming from repulsive bare interactions.

Rydberg atoms and Rydberg-dressed atoms haven long been recognized for their potential in quantum simulation and quantum information [10–14]. Recent experiments have successfully demonstrated a panoply of two-body interactions in cold gases of Rydberg-dressed alkali atoms [15–21]. In Rydberg dressing, the ground state atom (say n_0S) is weakly coupled to a Rydberg state (say nS or nD) with large principal number n by off-resonant light with Rabi frequency Ω and detuning Δ. The coupling can be achieved for example via a two-photon process involving an intermediate state n_1P to yield longer coherence times [22]. The huge dipole moments of the Rydberg states lead to strong interactions that exceed the natural van der Waals interaction by a factor that scales with powers of n [12, 13]. The interaction between two Rydberg-dressed atoms takes the following form [22]:

$$V(\mathbf{r}) = \frac{u_0}{r^6 + r_c^6}. \quad (1)$$

Here $r = |\mathbf{r}|$ is the inter-particle distance, $u_0 = (\Omega/2\Delta)^4 C_6$ is the interaction strength, C_6 is the van der Waals coefficient, and $r_c = |C_6/2\hbar\Delta|^{1/6}$ is the soft-core radius and the characteristic scale for the interaction range. As shown in Fig. 1, $V(\mathbf{r})$ has a step-like soft-core for $r \lesssim r_c$ before decaying to a van der Waals tail at long distances. Both u_0 and r_c can be tuned experimentally via Ω and Δ [22]. Moreover, by choosing proper Rydberg states (e.g. nS versus nD for ^{6}Li with $n > 30$ [23]) C_6 and u_0 can be made either repulsive or attractive. By choosing proper n, Δ and Ω, atom loss can be reduced to achieve a sufficiently long life time to observe many-body phenomena [18, 20, 22, 24].

Previous theoretical studies have explored the novel many-body phenomena associated with interaction Eq. (1) in bosonic [22, 25–31] and fermionic gases [24] including the prediction of topological superfluids [23] and topological density waves [32]. Here we consider single-component Rydberg Fermi gases confined in 2D [33], where mean-field and random phase approximation (RPA) become unreliable due to enhanced quantum fluctuations. Our goal is to set up a theory to systematically describe the competing many-body phases of 2D Rydberg-dressed Fermi gas by treating them on equal footing beyond the weak-coupling regime and RPA. We achieve this by solving the functional renormalization group flow equations for the fermionic interaction vertices. The resulting phase diagram (Fig. 2) is much richer than the RPA prediction [33] and reveals an unexpected f-wave phase.

The paper is organized as follows. In Sec. II we intro-

* xiaopeng_li@fudan.edu.cn

duce many-body phases of Rydberg-dressed Fermi gas within mean-field from the standard Cooper instability analysis and Random Phase Approximation. In Sec. III we present the numerical implementation of Functional Renormalization Group to this problem and in Sec. IV we show many-body phases beyond mean field calculation which manifest intertwined quantum fluctuations in pairing and density-wave channels. In Sec. V, we summarize our study and implications of our findings for future experimental developments in ultracold gases.

II. RYDBERG-DRESSED FERMI GAS

We first highlight the unique properties of Rydberg-dressed Fermi gas by comparing it with other well-known Fermi systems with long-range interactions such as the electron gas and dipolar Fermi gas. Correlations in electron liquid are characterized by a single dimensionless parameter r_s, the ratio of Coulomb interaction energy to kinetic energy. In the high density limit $r_s \ll 1$, the system is weakly interacting while in the low density limit $r_s \gg 1$, Wigner crystal is formed. The intermediate correlated regime with $r_s \sim 1$ can only be described by various approximations [34]. Similarly, dipolar Fermi gas also has a power-law interaction that lacks a scale, so a parameter analogous to r_s can be introduced which varies monotonically with the density [35]. The situation is different in Rydberg-dressed Fermi gas with interaction given by Eq. (1). From the inter-particle spacing $1/\sqrt{2\pi n}$ and the Fermi energy $\epsilon_F = 2\pi n/m$ (we put $\hbar = 1$ and $k_B = 1$) in terms of areal density n, one finds that the ratio of interaction energy to kinetic energy scales as $n^2/[1 + (2\pi r_c^2)^3 n^3]$, which varies non-monotonically with n unlike electron liquid due to r_c (Fig. 1a inset). Distinctive feature of the interaction $V(\mathbf{r})$ is revealed by its Fourier transform in 2D [33],

$$V(\mathbf{q}) = gG\left(q^6 r_c^6/6^6\right), \quad g = \pi u_0/3r_c^4, \tag{2}$$

where $\mathbf{q}$ is the momentum, $q = |\mathbf{q}|$, g is the coupling strength and G is the Meijer G-function [36]. The function $V(\mathbf{q})$, plotted in Fig. 1b, develops a negative minimum at $q = q_c \sim 4.82/r_c$. This is the momentum space manifestation of the step-like interaction potential Eq. (1). These unique behaviors are the main culprits of its rich phase diagram.

Starting from the free Fermi gas, increasing the interaction g may lead to a diverging susceptibility and drive the Fermi liquid into a symmetry-broken phase. We first give a qualitative discussion of potential ordered phases using standard methods to orient our numerical FRG results later. For attractive interactions, $u_0 < 0$, an arbitrarily small g is sufficient to drive the Cooper instability. By decomposing $V(\mathbf{q} = \mathbf{p}_F - \mathbf{p}'_F)$ into angular momentum channels, $V(2p_F \sin\frac{\theta}{2}) = \sum_\ell V_\ell e^{i\ell\theta}$ where θ is the angle between $\mathbf{p}_F$ and $\mathbf{p}'_F$, one finds different channels decouple and the critical temperature of the ℓ-th channel $T_c(\ell) \sim e^{-1/N_0 V_\ell}$ [37] with $N_0 = m/2\pi$ being the density of states. Thus the leading instability comes from the channel with the largest V_ℓ (hence the largest T_c). Fig. 1c illustrates $T_c(\ell)$ as a function of r_c for fixed p_F. It is apparent that the dominant instability is in the $\ell = \pm 1$ channel, i.e., p-wave pairing. Its T_c develops a dome structure and reaches maximum around $p_F r_c \approx 2$. For large r_c, higher angular momentum channels start to compete with the $\ell = \pm 1$ channel.

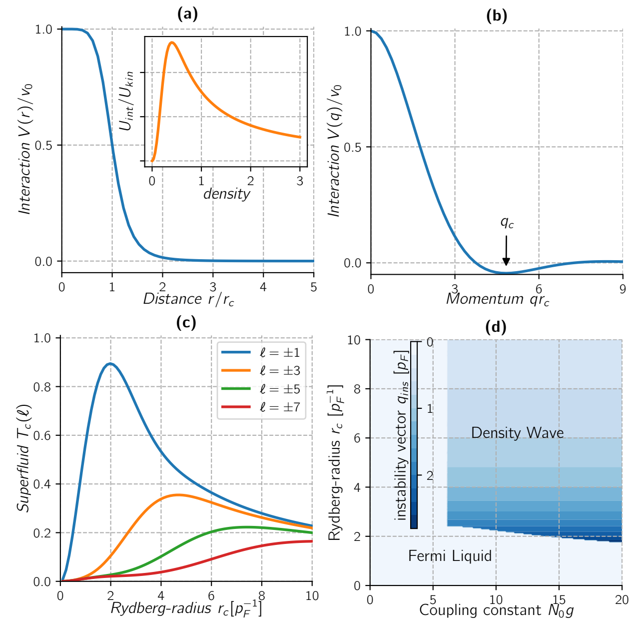

FIG. 1. Single-component Fermi gas with Rydberg-dressed interactions in 2D. (a) The interaction potential Eq. (1) shows a step-like soft core of radius r_c and a long-range tail. (Inset) Ratio of the interaction to kinetic energy varies non-monotonically with density. (b) The Rydberg-dressed interaction Eq. (2) in momentum space attains a negative minimum at $q_c \sim 4.82/r_c$. (c) For attractive interactions, the critical temperatures in different angular momentum ℓ channels (in arbitrary units) from the solution of the Cooper problem. The leading instability is p-wave, $\ell = \pm 1$. Maximum T_c is around $p_F r_c \approx 2$. (d) For repulsive interactions, random phase approximation points to a density-wave order. False color (shading) shows the ordering wave vector of density modulations.

For repulsive bare interactions, $u_0 > 0$, a sufficiently strong interaction g can induce an instability toward the formation of (charge) density waves. This has been shown recently [33] for 2D Rydberg-dressed Fermi gas using random phase approximation (RPA) which sums over a geometric series of "bubble diagrams" to yield the static dielectric function, $\epsilon(\mathbf{q}) = 1 - V(\mathbf{q})\chi_0(\mathbf{q})$ where the Linhard function $\chi_0(\mathbf{q}) = -N_0[1 - \Theta(q - 2k_F)\sqrt{q^2 - 4k_F^2}/q]$. The onset of density wave instability is signaled by $\epsilon(\mathbf{q}) = 0$ at some wave vector $q = q_{ins}$, i.e. the softening of particle-hole excitations. Within RPA, q_{ins} always coincides with q_c, and the resulting phase diagram is shown in Fig. 1d.

While these standard considerations capture the p-wave pairing and density wave order, they fail to describe the physics of intertwined scattering between particle-particle and particle-hole channels. We show below that this missing ingredient exhibits significant effects, leading to the emergence of a robust f-wave superfluid in the repulsive regime. For a detailed comparison between RPA and FRG see Ref. [38].

III. NUMERICAL IMPLEMENTATION OF FUNCTIONAL RENORMALIZATION GROUP

Functional renormalization group (FRG) is a powerful technique that can accurately predict the many-body instabilities of strongly interacting fermions [39]. It implements Wilson's renormalization group for interacting fermions in a formally exact manner by flowing the generating functional of the many-body system Γ as a sliding momentum scale Λ is varied. Starting from the bare interaction $V(\mathbf{q})$ at a chosen ultraviolet scale Λ_{UV}, higher energy fluctuations are successively integrated out to yield the self-energy Σ and effective interaction vertex Γ at a lower scale $\Lambda < \Lambda_{UV}$. As Λ is lowered toward a very small value Λ_{IR}, divergences in the channel coupling matrices and susceptibilities point to the development of long-range order. Its advantage is that all ordering tendencies are treated unbiasedly with full momentum resolution. The main draw back is its numerical complexity: at each RG step, millions of running couplings have to be retained. FRG has been applied to dipolar Fermi gas [38, 40] and extensively benchmarked against different techniques [41–44]. For more details about the formalism, see reviews [39] and [45]. Note that our system is a continuum Fermi gas, not a lattice system extensively studied and reviewed in [39].

The central task of FRG is to solve the coupled flow equations for self-energy $\Sigma_{1',1}$ and two-particle vertex $\Gamma_{1',2';1,2}$ [39]:

$$\partial_\Lambda \Sigma_{1',1} = -\sum_2 S_2 \Gamma_{1',2;1,2},$$
$$\partial_\Lambda \Gamma_{1',2';1,2} = \sum_{3,4} \Pi_{3,4}\Big[\frac{1}{2}\Gamma_{1',2';3,4}\Gamma_{3,4;1,2} - \Gamma_{1,'4;1,3}\Gamma_{3,2';4,2} + \Gamma_{2',4;1,3}\Gamma_{3,1';4,2}\Big], \quad (3)$$

Here the short-hand notation $1 \equiv (\omega_1, \mathbf{p}_1)$, $1, 2$ $(1', 2')$ label the incoming (outgoing) legs of the four-fermion vertex Γ, and the sum stands for integration over frequency and momentum, $\Sigma \to \int d\omega d^2\mathbf{p}/(2\pi)^3$. Diagrammatically, the first term in Eq. (3) is the BCS diagram in the particle-particle channel, and the second and third terms are known as the ZS and ZS' diagram in the particle-hole channel [46]. The polarization bubble $\Pi_{3,4} = G_3 S_4 + S_3 G_4$ contains the product of two scale-dependent Green functions defined by

$$G_{\omega,\mathbf{p}} = \frac{\Theta(|\xi_\mathbf{p}| - \Lambda)}{i\omega - \xi_\mathbf{p} - \Sigma_{\omega,\mathbf{p}}}, \qquad S_{\omega,\mathbf{p}} = \frac{\delta(|\xi_\mathbf{p}| - \Lambda)}{i\omega - \xi_\mathbf{p} - \Sigma_{\omega,\mathbf{p}}}. \quad (4)$$

Note that G, S, Σ and Γ all depend on the sliding scale Λ, we suppressed their Λ-dependence in equations above for brevity.

Several well-justified approximations are used to make the flow equations computationally tractable. To identify leading instabilities, the self-energy can be safely dropped, and the frequency dependence of Γ can be neglected [39]. As a result, the frequency integral of the fermion loops in Eq. (3) can be performed analytically. Furthermore, we retain the most relevant dependence of Γ on $\mathbf{p}$ by projecting all off-shell momenta radially onto the Fermi surface [39]. Then, Γ is reduced to $\Gamma_{1',2';1,2} \to \Gamma(\mathbf{p}'_{F1}, \mathbf{p}'_{F2}, \mathbf{p}_{F1})$ where the last momentum variable is dropped because it is fixed by conservation, and the subscript in $\mathbf{p}_F$ indicates radial projection onto the Fermi surface. The initial condition for Γ at the ultraviolet scale Λ_{UV} is given by the antisymmetrized bare interaction $V(\mathbf{q})$,

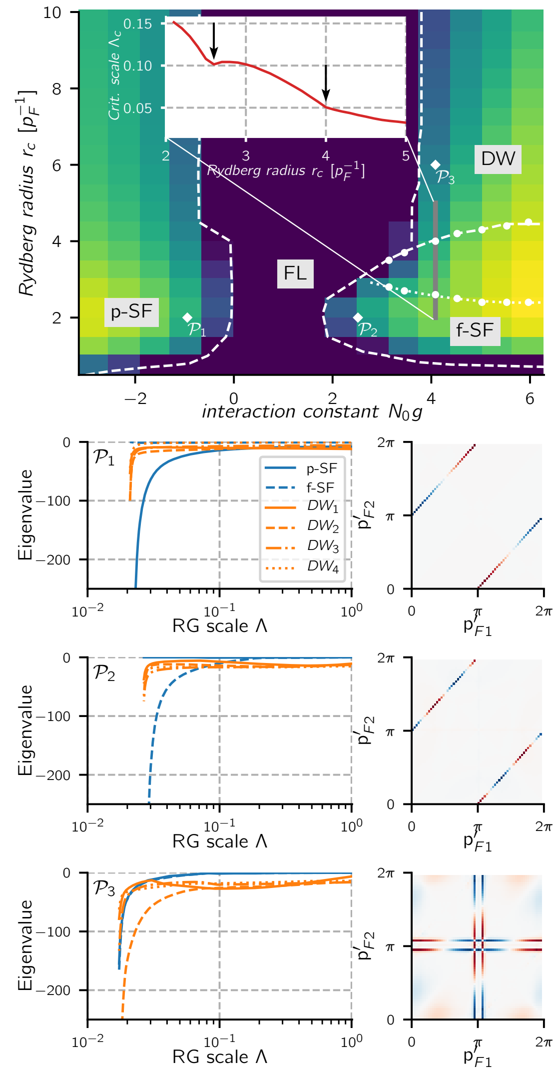

FIG. 2. Phase diagram of Rydberg-dressed spinless Fermi gas in 2D based on FRG. Tuning the interaction range r_c and interaction strength g yields Fermi Liquid (FL), p-wave superfluid (p-SF), f-wave superfluid (f-SF), and density-wave (DW). False color (shading) indicates the critical scale Λ_c of the instability where brighter (darker) regions have higher (lower) T_c. Panels labelled with $\mathcal{P}_1$, $\mathcal{P}_2$ and $\mathcal{P}_3$ show the details of renormalization flow and vertex function for points marked with white diamonds on the phase diagram. The leading eigenvalues for a few channels (see legends) are shown on the left. The maps of vertex function $\Gamma(\mathbf{p}'_{F1}, \mathbf{p}'_{F2}, \mathbf{p}_{F1})$ are shown on the right for fixed $\mathbf{p}_{F1} = (-p_F, 0)$. Superfluid (density wave) order displays diagonal (horizontal and vertical) correlations.

$$\Gamma(\mathbf{p}'_{F1}, \mathbf{p}'_{F2}, \mathbf{p}_{F1})\big|_{\Lambda_{UV}} \equiv \frac{1}{2}[V(\mathbf{p}'_{F1} - \mathbf{p}_{F1}) - V(\mathbf{p}'_{F2} - \mathbf{p}_{F1})]. \quad (5)$$

We solve the flow equation by the Euler method on a logarithmic grid of Λ consisting of 10^3 RG steps going from $\Lambda_{UV} = 0.99E_F$ down to $\Lambda_{IR} = 10^{-3}E_F$. Each $\mathbf{p}_F$ is discretized on an angular grid with up to hundreds of patches on the Fermi surface [47]. We monitor the flow of $\Gamma(\mathbf{p}'_{F1}, \mathbf{p}'_{F2}, \mathbf{p}_{F1})$ which contains hundreds of millions of running coupling constants. When the absolute value of a running coupling constant in Γ exceeds a threshold, e.g. $50E_F$, signaling an imminent divergence, we terminate the flow, record the critical scale Λ_c, and analyze the vertex to diagnose the instability. If the flow continues smoothly down to Λ_{IR}, we conclude the Fermi liquid is stable down to exponentially small temperatures. Scanning the parameter space (g, r_c) gives the phase diagram, whereas Λ_c provides a rough estimate of the T_c of each ordered phase.

Two complementary methods are employed to identify the leading instability from the large, complex data set of Γ. First, we plot $\Gamma(\mathbf{p}'_{F1}, \mathbf{p}'_{F2}, \mathbf{p}_{F1})$ at Λ_c against the angular directions of $\mathbf{p}'_{F1}$ and $\mathbf{p}'_{F2}$ for fixed $\mathbf{p}_{F1} = (-p_F, 0)$ [48] to reveal the dominant correlations between particles on the Fermi surface. The color map (Fig. 2, lower right columns) shows diagonal structures ($\mathbf{p}'_{F1} = -\mathbf{p}'_{F2}$) for pairing instability, and horizontal-vertical structures (scattering $\mathbf{p}_{F1} \to \mathbf{p}'_{F1}$ with momentum transfer close to 0 or $2p_F$) for density waves [45, 49]. This method directly exposes the pairing symmetry through the number of nodes along the diagonal structures: a p-wave phase has one node, and an f-wave phase has three nodes, etc. In the second method, we construct the channel matrices from Γ, e.g. $V_{BCS}(\mathbf{p}', \mathbf{p}) = \Gamma(\mathbf{p}', -\mathbf{p}', \mathbf{p})$ for the pairing channel, and $V^{\mathbf{q}}_{DW}(\mathbf{p}', \mathbf{p}) = \Gamma(\mathbf{p} + \mathbf{q}/2, \mathbf{p}' - \mathbf{q}/2, \mathbf{p} - \mathbf{q}/2)$ for the density wave channel. Different values of $\mathbf{q}$, e.g. $\mathbf{q}_i = (q_i, 0)$ with $q_i \in \{0.05p_F, 0.5p_F, p_F, 2p_F\}$ for $i \in \{1, ..., 4\}$ respectively, are compared (see DW_i in Fig. 2, left column). The channel matrices are then diagonalized and their the most negative eigenvalues are monitored. This method provides a clear picture of the competition among the channels. The eigenvector of the leading divergence exposes the orbital symmetry, e.g. p- or f-wave, of the incipient order.

IV. PHASE DIAGRAM FROM FRG

The resulting phase diagram is summarized in the top panel of Fig. 2. In addition to the Fermi liquid, three ordered phases are clearly identified. Here the filled circles mark the phase boundary, the color indicates the critical scales Λ_c which is proportional to T_c [39], and the dash lines are guide for the eye and they roughly enclose the regions where Λ_c is higher than the numerical IR scale Λ_{IR}. For attractive interactions $g < 0$, e.g. at the point $\mathcal{P}_1$, the leading eigenvalues are from V_{BCS} and doubly degenerate with p-wave symmetry. The vertex map also reveals diagonal structures with single node (Fig. 2), confirming a p-wave superfluid phase. While the FRG here cannot directly access the wavefunction of the broken symmetry phase, mean field argument favors a $p_x + ip_y$ ground state because it is fully gapped and has the most condensation energy. Thus Rydberg-dressed Fermi gas is a promising system to realize the $p_x + ip_y$ topological superfluid. Our analysis suggests that the optimal T_c is around $p_F r_c \sim 2$ and T_c increases with $|u_0|$.

For repulsive interactions $g > 0$, which channel gives the leading instability depends intricately on the competition between p_F and r_c. **(a)** First, FRG reveals a density wave phase for $p_F r_c \gtrsim 4$, in broad agreement with RPA. For example, at point $\mathcal{P}_3$, the most diverging eigenvalue comes from V_{DW}, and the vertex map shows clear horizontal-vertical structures (Fig. 2). Note the separations between the horizontal/vertical lines, and relatedly the ordering wave vector, depend on r_c. **(b)** For $p_F r_c \lesssim 4$, however, the dominant instability comes from the BCS channel despite that the bare interaction is purely repulsive in real space. In particular, for small $p_F r_c \lesssim 2$, such as the point $\mathcal{P}_2$ in Fig. 2, the pairing symmetry can be unambiguously identified to be f-wave: the vertex map has three nodes, the most diverging eigenvalues of V_{BCS} are doubly degenerate, and their eigenvectors follow the form $e^{\pm i3\theta}$. This f-wave superfluid is the most striking result from FRG. **(c)** For $p_F r_c$ roughly between 2 and 4, sandwiched between the density wave and f-wave superfluid, lies a region where the superfluid paring channel strongly intertwines with the density wave channel. While the leading divergence is still superfluid, it is no longer pure f-wave, and it becomes increasingly degenerate with a subleading density wave order. This hints at a coexistence of superfluid and density wave.

To determine the phase boundary, we trace the evolution of Λ_c along a few vertical cuts in the phase diagram, and use the kinks in Λ_c as indications for the transition between the density wave and superfluid phase, or a change in pairing symmetry within the superfluid (see inset, top panel of Fig. 2). We have checked the phase boundary (filled circles) determined this way is consistent with the eigenvalue flow and vertex map.

Cooper pairing can occur in repulsive Fermi liquids via the Kohn-Luttinger (KL) mechanism through the renormalization of fermion vertex by the particle-hole fluctuations. Even for featureless bare interactions $V(\mathbf{q}) = U > 0$, the effective interaction V_ℓ in angular momentum channel ℓ can become attractive due to over-screening by the remaining fermions [50]. In 2D, the KL mechanism becomes effective at higher orders of perturbation theory, e.g. U^3, and the leading pairing channel is believed to be p-wave [51]. Here, the effective interaction is also strongly renormalized from the bare interaction by particle-hole fluctuations. We have checked that turning off the ZS and ZS' channels eliminates superfluid order on the repulsive side. However, our system exhibits f-wave pairing with a significant critical temperature in contrast to usual KL mechanism with exponentially small T_c. This is because the Rydberg-dressed interaction already contains a "pairing seed": $V(\mathbf{q})$ develops a negative minimum in momentum space for $q = q_c$ unlike the featureless interaction U. Among all the scattering processes $(\mathbf{p}_F, -\mathbf{p}_F) \to (\mathbf{p}'_F, -\mathbf{p}'_F)$, those with $q = |\mathbf{p}'_F - \mathbf{p}_F| \sim q_c$ favor pairing. It follows that pairing on the repulsive side occurs most likely when the Fermi surface has a proper size, roughly $2p_F \sim q_c$, in broad agreement with the FRG phase diagram. These considerations based on the bare interaction and BCS approach, however, are insufficient to explain the f-wave superfluid revealed only by FRG, which accurately accounts the interference between the particle-particle and particle-hole channels. The pairing seed and over screening conspire to give rise to a robust f-wave superfluid with significant T_c.

V. CONCLUSION

We developed an unbiased numerical technique based on FRG to obtain the phase diagram for the new system of Rydberg-dressed Fermi gas to guide future experiment. We found an f-wave superfluid with unexpectedly high T_c driven by repulsive interactions beyond the conventional Kohn-Luttinger paradigm. The physical mechanism behind the T_c enhancement is traced back to the negative minimum in the bare interaction, as well as the renormalization of the effective interaction by particle-hole fluctuations. These results contribute to our understanding of unconventional pairing from repulsive interactions, and more generally, competing many-body instabilities of fermions with long-range interactions. Our analysis may be used for optimizing T_c by engineering effective interactions using schemes similar to Rydberg dressing. Our FRG approach can also be applied to illuminate the rich interplay of competing density wave and pairing fluctuations in solid state correlated quantum materials. Note that f-wave pairing has been previously discussed in the context of fermions on the p-orbital bands [52, 53].

ACKNOWLEDGMENTS

This work is supported by NSF Grant No. PHY-1707484, AFOSR Grant No. FA9550-16-1-0006 (A.K. and E.Z.), ARO Grant No. W911NF-11-1-0230, and MURI-ARO Grant No. W911NF-17-1-0323 (A.K.). X.L. acknowledges support by National Program on Key Basic Research Project of China under Grant No. 2017YFA0304204 and National Natural Science Foundation of China under Grants No. 11774067.

[1] P. A. Lee, N. Nagaosa, and X.-G. Wen, "*Doping a Mott insulator: Physics of high-temperature superconductivity*," Rev. Mod. Phys. **78**, 17–85 (2006).

[2] Andrew Peter Mackenzie and Yoshiteru Maeno, "*The superconductivity of* Sr_2RuO_4 *and the physics of spin-triplet pairing*," Rev. Mod. Phys. **75**, 657–712 (2003).

[3] G. R. Stewart, "*Superconductivity in iron compounds*," Rev. Mod. Phys. **83**, 1589–1652 (2011).

[4] Stefano Giorgini, Lev P. Pitaevskii, and Sandro Stringari, "*Theory of ultracold atomic Fermi gases*," Rev. Mod. Phys. **80**, 1215–1274 (2008).

[5] W. Ketterle and M. W. Zwierlein, "*Making, probing and understanding ultracold Fermi gases*," arXiv:0801.2500 (2008).

[6] R. A. Hart *et al.*, "*Observation of antiferromagnetic correlations in the Hubbard model with ultracold atoms*," Nature **519**, 211 (2015).

[7] A. Mazurenko *et al.*, "*A cold-atom Fermi–Hubbard antiferromagnet*," Nature **545**, 462 (2017).

[8] Peter T Brown *et al.*, "*Bad metallic transport in a cold atom Fermi-Hubbard system*," Science **363**, 379–382 (2019).

[9] I. Bloch, J. Dalibard, and W. Zwerger, "*Many-body physics with ultracold gases*," Rev. Mod. Phys. **80**, 885–964 (2008).

[10] H. Weimer, M. Müller, I. Lesanovsky, P. Zoller, and H. P. Büchler, "*A Rydberg quantum simulator*," Nat. Phys. **6**, 382–388 (2010).

[11] M. D. Lukin, M. Fleischhauer, R. Cote, L. M. Duan, D. Jaksch, J. I. Cirac, and P. Zoller, "*Dipole Blockade and Quantum Information Processing in Mesoscopic Atomic Ensembles*," Phys. Rev. Lett. **87**, 037901 (2001).

[12] M. Saffman, T. G. Walker, and K. Mølmer, "*Quantum information with Rydberg atoms*," Rev. Mod. Phys. **82**, 2313–2363 (2010).

[13] A. Browaeys and T. Lahaye, "*Interacting cold Rydberg atoms: A toy many-body system*," Prog. Math. Phys. **68**, 177–198 (2016).

[14] T. Karpiuk et al., "*Imaging single Rydberg electrons in a Bose-Einstein condensate*," New Journal of Physics **17**, 053046 (2015).

[15] P. Schauß, J. Zeiher, T. Fukuhara, S. Hild, M. Cheneau, T. Macrì, T. Pohl, I. Bloch, and C. Groß, "*Crystallization in Ising quantum magnets*," Science **347**, 1455–1458 (2015).

[16] J. Zeiher, R. Van Bijnen, P. Schauß, S. Hild, J. Choi, T. Pohl, I. Bloch, and C. Gross, "*Many-body interferometry of a Rydberg-dressed spin lattice*," Nature Physics **12**, 1095 (2016).

[17] Simon Hollerith *et al.*, "*Quantum gas microscopy of Rydberg macrodimers*," arXiv:1812.07533 (2018).

[18] Johannes Zeiher, Jae-yoon Choi, Antonio Rubio-Abadal, Thomas Pohl, Rick van Bijnen, Immanuel Bloch, and Christian Gross, "*Coherent Many-Body Spin Dynamics in a Long-Range Interacting Ising Chain*," Phys. Rev. X **7**, 041063 (2017).

[19] Y.-Y. Jau, A. M. Hankin, T. Keating, I. H. Deutsch, and G. W. Biedermann, "*Entangling atomic spins with a Rydberg-dressed spin-flip blockade*," Nature Physics **12**, 71–74 (2015).

[20] Elmer Guardado-Sanchez, Peter T. Brown, Debayan Mitra, Trithep Devakul, David A. Huse, Peter Schauß, and Waseem S. Bakr, "*Probing the Quench Dynamics of Antiferromagnetic Correlations in a 2D Quantum Ising Spin System*," Phys. Rev. X **8**, 021069 (2018).

[21] Victoria Borish, Ognjen Markovi, Jacob A. Hines, Shankari V. Rajagopal, and Monika Schleier-Smith, "*Transverse-Field Ising Dynamics in a Rydberg-Dressed Atomic Gas*," (2019), arXiv:1910.13687.

[22] N. Henkel, R. Nath, and T. Pohl, "*Three-Dimensional Roton Excitations and Supersolid Formation in Rydberg-Excited Bose-Einstein Condensates*," Phys. Rev. Lett. **104**, 195302 (2010).

[23] B. Xiong, H. H. Jen, and D.W. Wang, "*Topological superfluid by blockade effects in a Rydberg-dressed Fermi gas*," Phys. Rev. A **90**, 013631 (2014).

[24] W. H. Li, T. C. Hsieh, C. Y. Mou, and D. W. Wang, "*Emergence of a Metallic Quantum Solid Phase in a Rydberg-Dressed Fermi Gas*," Phys. Rev. Lett. **117**, 035301 (2016).

[25] F. Maucher, N. Henkel, M. Saffman, W. Królikowski, S. Skupin, and T. Pohl, "*Rydberg-Induced Solitons: Three-Dimensional Self-Trapping of Matter Waves*," Phys. Rev. Lett. **106**, 170401 (2011).

[26] A. W. Glaetzle, M. Dalmonte, R. Nath, I. Rousochatzakis, R. Moessner, and P. Zoller, "*Quantum Spin-Ice and Dimer Models with Rydberg Atoms*," Phys. Rev. X **4**, 041037 (2014).

[27] I. Seydi, S. H. Abedinpour, R. E. Zillich, R. Asgari, and B. Tanatar, "*Rotons and Bose condensation in Rydberg-dressed Bose Gases*," arXiv:1905/01643 (2019).

[28] G. Pupillo, A. Micheli, M. Boninsegni, I. Lesanovsky, and P. Zoller, "*Strongly Correlated Gases of Rydberg-Dressed Atoms: Quantum and Classical Dynamics*," Phys. Rev. Lett. **104**, 223002 (2010).
[29] N. Henkel, F. Cinti, P. Jain, G. Pupillo, and T. Pohl, "*Supersolid Vortex Crystals in Rydberg-Dressed Bose-Einstein Condensates*," Phys. Rev. Lett. **108**, 265301 (2012).
[30] Guido Masella, Adriano Angelone, Fabio Mezzacapo, Guido Pupillo, and Nikolay V. Prokof'ev, "*Supersolid Stripe Crystal from Finite-Range Interactions on a Lattice*," Phys. Rev. Lett. **123**, 045301 (2019).
[31] Stefano Rossotti, Martina Teruzzi, Davide Pini, Davide Emilio Galli, and Gianluca Bertaina, "*Quantum Critical Behavior of One-Dimensional Soft Bosons in the Continuum*," Phys. Rev. Lett. **119**, 215301 (2017).
[32] X. Li and S. Das Sarma, "*Exotic topological density waves in cold atomic Rydberg-dressed fermions*," Nat. Commun. **6**, 7137 (2015).
[33] R. Khasseh, S. H. Abedinpour, and B. Tanatar, "*Phase diagram and dynamics of Rydberg-dressed fermions in two dimensions*," Phys. Rev. A **96**, 053611 (2017).
[34] P. Nozieres and D. Pines, *Theory Of Quantum Liquids (Frontiers in Physics) (v. 1 & 2)* (Westview Press, 1999).
[35] M. A. Baranov, M. Dalmonte, G. Pupillo, and P. Zoller, "*Condensed Matter Theory of Dipolar Quantum Gases*," Chem. Rev. **112**, 5012–5061 (2012).
[36] In Mathematica, this Meijer G-function is called with `MeijerG[{{},{}},{{0,1/3,2/3,2/3},{0,1/3}},`$z^6/6^6$`]` where $z = qr_c$.
[37] V. P. Mineev and K. Samokhin, *Introduction to Unconventional Superconductivity* (CRC Press, 1999).
[38] Ahmet Keleş and Erhai Zhao, "*Competing many-body instabilities in two-dimensional dipolar Fermi gases*," Phys. Rev. A **94**, 033616 (2016).
[39] W. Metzner, M. Salmhofer, C. Honerkamp, V. Meden, and K. Schönhammer, "*Functional renormalization group approach to correlated fermion systems*," Rev. Mod. Phys. **84**, 299–352 (2012).
[40] S. G. Bhongale, L. Mathey, Shan-Wen Tsai, Charles W. Clark, and Erhai Zhao, "*Bond Order Solid of Two-Dimensional Dipolar Fermions*," Phys. Rev. Lett. **108**, 145301 (2012).
[41] L. M. Sieberer and M. A. Baranov, "*Collective modes, stability, and superfluid transition of a quasi-two-dimensional dipolar Fermi gas*," Phys. Rev. A **84**, 063633 (2011).
[42] M. M. Parish and F. M. Marchetti, "*Density Instabilities in a Two-Dimensional Dipolar Fermi Gas*," Phys. Rev. Lett. **108**, 145304 (2012).
[43] M. Babadi and E. Demler, "*Density ordering instabilities of quasi-two-dimensional fermionic polar molecules in single-layer and multilayer configurations: Exact treatment of exchange interactions*," Phys. Rev. B **84**, 235124 (2011).
[44] Z. Wu, J. K. Block, and G. M. Bruun, "*Coexistence of density wave and superfluid order in a dipolar Fermi gas*," Phys. Rev. B **91**, 224504 (2015).
[45] P. Kopietz, L. Bartosch, and Schutz F., *Introduction to the Functional Renormalization Group (Lecture Notes in Physics)* (Springer, 2010).
[46] R. Shankar, "*Renormalization-group approach to interacting fermions*," Rev. Mod. Phys. **66**, 129–192 (1994).
[47] To speed up the calculation, the FRG algorithm is adapted to run parallel on Graphic Processing Units.
[48] This is done without loss of generality due to the rotational invariance.
[49] C. Honerkamp, M. Salmhofer, N. Furukawa, and T. M. Rice, "*Breakdown of the Landau-Fermi liquid in two dimensions due to umklapp scattering*," Phys. Rev. B **63**, 035109 (2001).
[50] W. Kohn and J. M. Luttinger, "*New Mechanism for Superconductivity*," Phys. Rev. Lett. **15**, 524–526 (1965).
[51] A. V. Chubukov, "*Kohn-Luttinger effect and the instability of a two-dimensional repulsive Fermi liquid at T=0*," Phys. Rev. B **48**, 1097–1104 (1993).
[52] Wei-Cheng Lee, Congjun Wu, and S. Das Sarma, "*F-wave pairing of cold atoms in optical lattices*," Phys. Rev. A **82**, 053611 (2010).
[53] Hsiang-Hsuan Hung, Wei-Cheng Lee, and Congjun Wu, "*Frustrated Cooper pairing and f-wave supersolidity in cold-atom optical lattices*," Phys. Rev. B **83**, 144506 (2011).